Immunogenicity landscape of cytotoxic T lymphocyte epitopes in sequence space.

Authors: Masato Ogishi[1*] and Hiroshi Yotsuyanagi[1]

Affiliations:

[1] Department of Infectious Diseases and Applied Immunology, Research Hospital, The Institute of Medical Science, The University of Tokyo, Tokyo, 108-0071, Japan

* To whom correspondence should be addressed: Masato Ogishi (oogishi-tky@umin.ac.jp)

Keywords: Epitope immunogenicity prediction, human leucocyte antigen class I, T cell receptor, escape, neoepitope

Abstract

Cytotoxic T lymphocytes (CTLs) recognize peptides known as epitopes presented onto MHC-I molecules to trigger an immune response. However, factors demarcating epitopes from non-immunogenic MHC binders remain poorly understood. Here, using 21,146 human MHC-I-loaded peptide sequences, we demonstrated an accurate immunogenicity prediction through a sequence-based approximation of the contact potential profiles (CPPs) of peptides against pooled TCR repertoires in conjunction with MHC binding information, achieving the area under the curve (AUC) of 79%. Predictive features provided insights into molecular scanning by TCR repertoire. Our framework also worked for primate and mouse peptide datasets. The quantitative immunogenicity scores delineated the landscapes of viral escaping and epitope formation through epitope mapping in sequence space and predicted overall survivals of cancer patients in checkpoint blockade cohorts. Overall, our analysis provides insights into the high-dimensional architectures of CTL activation and expedites translational efforts toward precision immunotherapy in infectious diseases and cancer.

Introduction

Adaptive immunity is triggered by antigens. Antigens are processed into peptide fragments by proteasomes, transported into the endoplasmic reticulum, and coupled to major histocompatibility complex [MHC; also called the human leukocyte antigen (HLA) in humans] molecules on the surface of antigen-presenting cells (APCs). Naïve T cells interact with MHC-loaded peptides via their receptor (T cell receptor, TCR), and successful recognition activates them to initiate subsequent immunological orchestration[1]. The term "epitope" means an immunogenic MHC-loaded peptide. However, strong MHC binding does not ensure immunogenicity, and vice versa[2–4]. Although antigen processing and MHC binding have been successfully predicted[5,6], prediction of immunogenicity remains a challenging task to date[7–10].

Why not all MHC binders subject to TCR recognition serve as epitopes? Since immunogenicity is a product of the amplitude of MHC-loaded peptides and the likelihood of recognition by T cells[11,12], not only the interactions between the peptide and MHC molecule but also the recognition of the peptide-MHC complex by TCRs are the critical determinants of immunogenicity[13,14]. In this context, we hypothesized that the intermolecular contact potential profiles (CPPs) between MHC-loaded peptides and the host TCR repertoire would serve as predictive features of immunogenicity. Because

49 of the extreme diversity of TCR repertoire, neither *in vitro* assay nor structural modeling
50 is a feasible approach. Instead, we hereby established an alternative, sequence-based
51 framework which we termed Repitope, approximating the CPPs using amino acid
52 pairwise contact potential (AACP) scales. We made three assumptions. First, only a
53 small fraction of TCRs in the host TCR repertoire recognize a given MHC-loaded
54 peptide. Second, CDR3 loops, which exhibit the highest degree of genetic variability,
55 are sufficient in modeling the TCR-peptide interactions. Finally, only a small part of a
56 CDR3 loop interacts with a small part of a given peptide. With those assumptions in
57 mind, molecular scanning by the host TCR repertoire can be viewed as a parallelized
58 pairwise sequence alignment problem between peptide sequences and CDR3 fragment
59 sequences, with alignment scores calculated from AACP-derived custom substitution
60 matrix as surrogate measurements of inter-fragment contact potentials.

61 With the Repitope framework, we demonstrated an accurate and quantitative
62 prediction of immunogenicity of cytotoxic T lymphocyte (CTL) epitopes presented on
63 human HLA class I molecules. Incorporation of binding to representative HLA
64 supertypes improved the overall predictive accuracy, indicating the complementary
65 roles of HLA restriction and TCR recognition. The most predictive features provided
66 mechanistic insights into CTL immunity. Mapping adjacent peptides in sequence space

enabled prediction of bidirectional immune transitions including escaping and epitope formation. *In silico* mutagenesis followed by neighbor network clustering analysis enabled identification of transition-prone peptides after single amino acid substitutions. Finally, we demonstrated stratification of long-surviving patients treated with checkpoint inhibitors in melanoma and lung carcinoma cohorts from the accumulation of changes in immunogenicity between wild-type and mutated peptides. Collectively, our findings theoretically bolster our understanding of CTL immunity and galvanize the rational design of precision immunotherapy. We distributed datasets and essential functions as the R package *Repitope* (https://github.com/masato-ogishi/Repitope/) for ensuring reproducibility and warranting prospective validations in independent cohorts.

Results

Immunogenicity prediction from TCR-peptide contact potential profiling

We first collected a set of 21,146 peptides of lengths 8 to 11 amino acids with known HLA restrictions and T cell functional assay results from the Immune Epitope Database (IEDB)[15] and other literature[8,9,16–21], yielding 6,942 immunogenic epitopes and 14,204 non-immunogenic MHC binders. Experimentally verified HLA genotype and serotype information was integrated as HLA restriction (**Figure 1a** and **Supplementary Table 1** and **Methods**), against which prediction by NetMHC 4.0[6] showed stronger binding than non-restricting HLAs (**Figure 1b**). Meanwhile, epitopes showed significantly stronger binding than mere MHC binders (**Figure 1c**). Tumor neoepitopes showed at least comparable binding compared to virus-derived epitopes (**Figure 1d**).

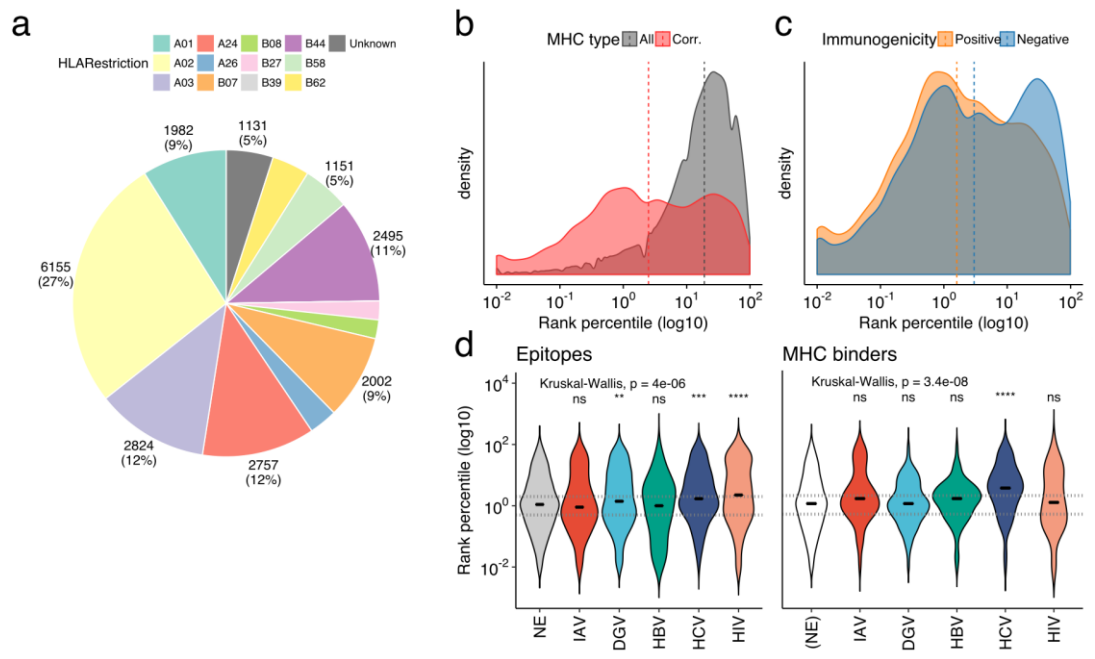

Figure 1. MHC binding prediction. (a) The distribution of restricting HLA supertypes in our metadataset. (b) The distributions of predicted rank percentiles. Binding was predicted using NetMHC 4.0 with default settings. Red, corresponding HLAs. Grey, all of the twelve HLA representatives [A1, A2, A3, A24, A26, B7, B8, B27, B39, B44, B58, and B62]. (c) The distributions of predicted rank percentiles between epitopes and non-immunogenic MHC binders. (d) The distributions of predicted rank percentiles in epitopes and MHC binders of various sources. NE, tumor neoepitope. IAV, influenza A virus. DGV, dengue virus. HBV, hepatitis B virus. HCV, hepatitis C virus. HIV, human immunodeficiency virus type 1. Neoepitope and viral data were obtained from TANTIGEN and IEDB database, respectively. In the right panel, tumor neoepitopes were depicted the same as the left panel for comparative purposes. Grey dashed line indicates the threshold of strong binders (0.5%). *P* values were calculated by Kruskal-Wallis test followed by Wilcoxon rank sum test with false discovery rate (FDR)-adjustment. **, $p < 0.01$; ***, $p < 0.001$; ****, $p < 0.0001$; ns, not significant.

As expected, previously reported tools for immunogenicity prediction showed only marginal predictive capabilities (**Supplementary Figure 1**). To achieve accurate immunogenicity prediction, we hereby propose the concept of TCR-peptide contact potential profiling (CPP) (**Figure 2a**). We extracted and pooled human TCR β CDR3 sequences from datasets deposited in the Sequence Read Archive using MiXCR

94 software[22]. CPP features were calculated against the fragment libraries generated from

95 pooled CDR3 sequences, with the fragment size ranging from 3 to 8. The depth of

96 fragment library was set 10,000 from preliminary experiments (**Supplementary Figure**

97 **2**). Iterative feature selection reduced the number of features down to 62

98 (**Supplementary Figure 3**). Heatmap analysis showed that immunogenic peptides were

99 clustered based on these features (**Figure 2b**).

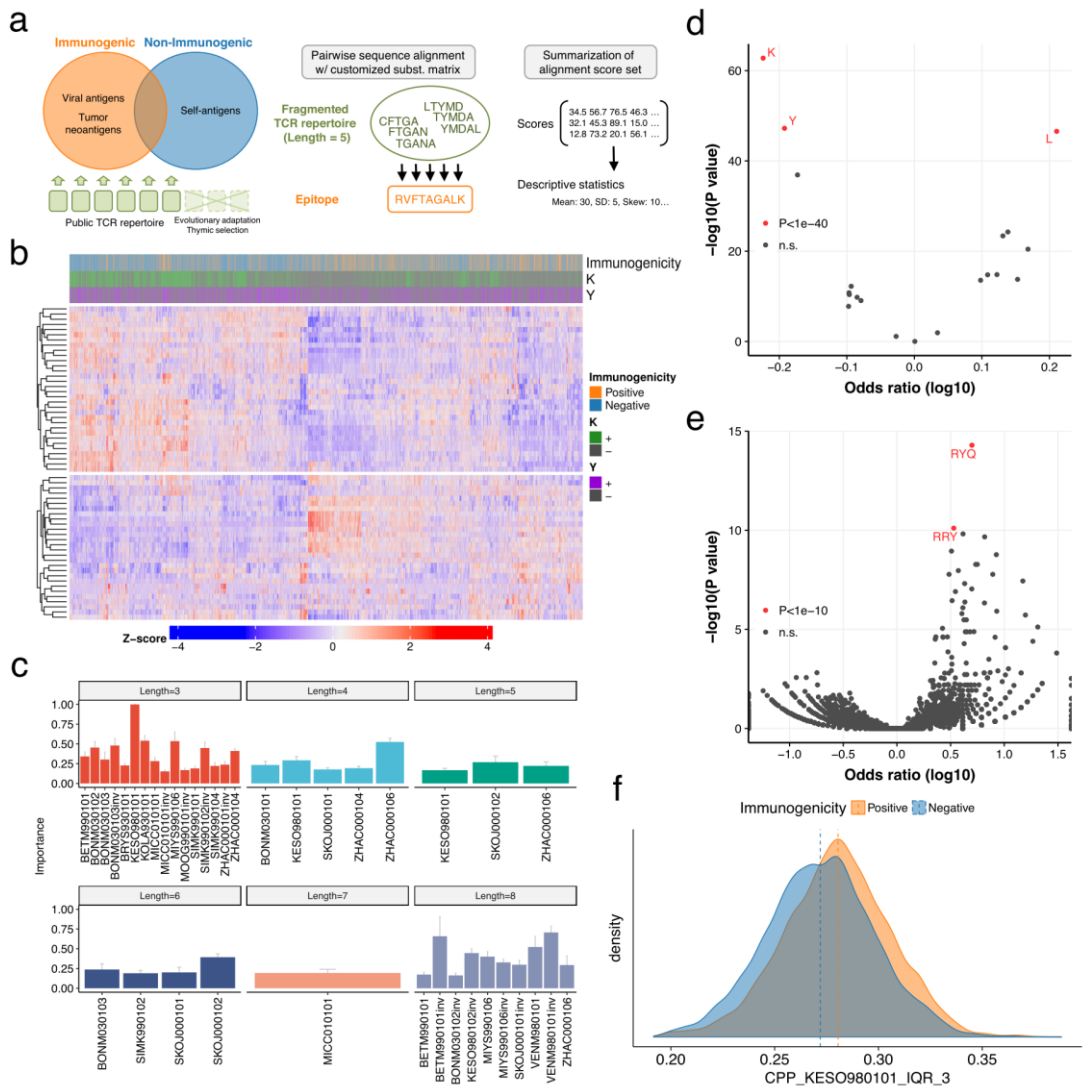

Figure 2. TCR-peptide contact potential profiling (CPP). (a) The concept of CPP. (b) Heatmap clustering analysis. (c) Feature importance analysis. Calculations were iterated five times with different random seeds. Bars represent mean and sd. (d-e) Residue/motif enrichment analysis. The volcano plots show the odds ratios and FDR-adjusted *p* values by chi-squared test from MHC binders to epitopes for each of the specified (d) residues and (e) motifs. (f) Distributions of the most predictive CPP feature.

The predictive features are likely to reflect the underlying mechanisms of molecular scanning of MHC-loaded peptides by the host TCR repertoire. Feature importance analysis suggested that CPP features derived from the fragment library of

103 length 3 played vital roles (**Figure 2c**). Also notably, the existence of residues K and Y
104 was indicated as essential features (**Supplementary Figure 3**). indeed, both residues
105 were more enriched to MHC binders (**Figure 2d**). In contrast, RYQ and other trimer
106 sequence motifs were enriched toward epitopes (**Figure 2e**). Given that nonamer
107 peptides bound to MHC class II are required to share only five residues to bind the same
108 TCR[23], and that MHC-I presents peptides shorter than MHC-II, it is likely that trimer
109 motifs are critical for at least the initial phase of molecular scanning by TCRs.
110 Moreover, the AACP scale KESO980101[24], which represents the transfer energy
111 derived from interfacial regions of protein-protein complexes and thus a plausible
112 metric of TCR-peptide interactions, consisted of the most predictive feature (**Figure 2f**
113 and **Supplementary Figure 3**).

114 By integrating physicochemical peptide descriptors, CPP features, and HLA
115 restrictions, we established a framework for immunogenicity prediction, which we
116 termed Repitope. Incorporation of either annotation-based HLA restrictions or binding
117 prediction results against twelve HLA representatives by NetMHC 4.0[6] improved
118 predictive performance (**Supplementary Figure 4**). Although annotation-based
119 predictions slightly outperformed those utilizing predicted binding categories, we
120 adopted the latter as "immunogenicity scores" for subsequent analyses (**Figure 3a, b**).

This makes the entire framework dependent solely on input peptide sequences. The classification of epitopes and MHC binders via immunogenicity score yields sensitivity and specificity of 70% and 73%, respectively, with the best score threshold being 0.35. The overall accuracy, kappa, and area under the curve (AUC) were 72%, 41%, and 79%, respectively (**Table 1**). The high predictive performance was retained across peptide lengths and HLA supertypes (**Supplementary Figure 5**). Reduction of the number of CPP features down to 14 still yielded AUC of 76% (**Supplementary Figure 6**). However, sequence-level peptide clustering led to slightly lower AUCs (**Supplementary Figure 7**). Furthermore, we found that either our framework or the prediction models constructed on the human peptide dataset successfully predicted immunogenicity for the peptide datasets of other species (**Supplementary Figure 8**). Particularly, immunogenicity scores calculated on the primate peptides using human models without HLA information yielded AUC of 70%. This finding implies the existence of shared regulatory mechanisms of CTL immunity between human and other primates. Predictive performances of various algorithms and conditions tested were summarized in **Table 1**.

In contrast to HLA binding, tumor neoepitopes exhibited significantly lower immunogenicity scores compared to epitopes of various viral origins (**Figure 1c** and

139 **Figure 3c**), with some exceptions such as gp100$_{280\text{-}288}$ (score = 0.85) and NY-ESO-1$_{157–}$
140 $_{165}$ (score = 0.70). This is consistent with previous observations that neoepitopes
141 dissimilar to self and similar to pathogen-derived epitopes are more likely to be
142 immunogenic[25].

143 Collectively, the aforementioned observations strongly suggest that the Repitope
144 framework recapitulates the high-dimensional architectures of CTL immunity to enable
145 *in silico* prediction of epitope immunogenicity.

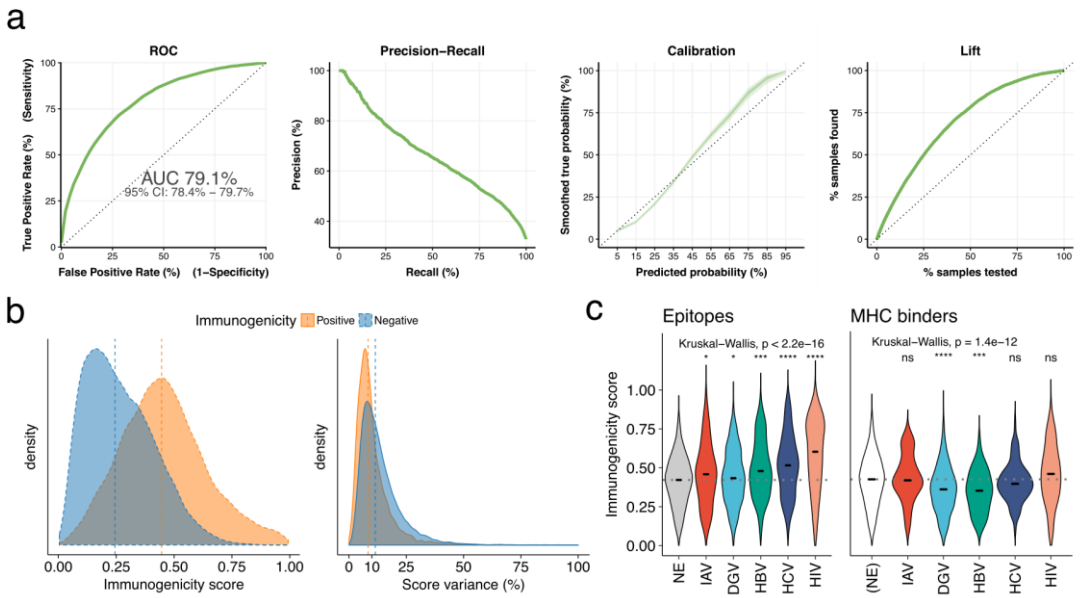

Figure 3. Immunogenicity prediction. (a-b) Immunogenicity scores. Probabilities were estimated from the most predictive 62 CPP features and predicted binding categories against twelve HLA representatives by NetMHC 4.0 (see **Supplementary Figure 3** and **Methods**). (a) Evaluation of immunogenicity scores. (b) Distributions of immunogenicity scores. Left, averaged scores. Right, coefficients of variance of scores between iterations. (c) The distributions of scores in epitopes and MHC binders of various sources. Grey dashed line indicates the median immunogenicity score in the tumor neoepitope dataset. See the legend of **Figure 1d** for data sources. *P* values were calculated by Kruskal-Wallis test followed by Wilcoxon rank sum test with FDR adjustment; *, $p < 0.05$; ***, $p < 0.001$; ****, $p < 0.0001$; ns, not significant.

146

Table 1. Summary of immunogenicity prediction results. Bolded was the prediction adopted as immunogenicity score. HLA, whether annotated HLA binding information or predicted binding by NetMHC 4.0 was used for machine learning. N_Feat, The number of CPP features (excluding HLA-related features) used. N_Pept, the number of peptides for machine learning. N_Epi, the number of epitopes in the dataset. ROC-AUC, the area under the receiver-operating curve. PRC-AUC, the area under the precision-recall curve. Thr, the best threshold determined from ROC. Acc, accuracy. Kap, Kappa coefficient. Sen, sensitivity. Spe, specificity. PPV, positive predictive value. NPV, negative predictive value. Prec, precision. Rec, recall.

Experiment ID	Data	HLA	N_Feat	N_Pept	N_Epi	ROC-AUC	PRC-AUC	Thr	Acc	Kap	Sen	Spe	PPV	NPV	Prec	Rec
IEDB	Human	n.a.	n.a.	21,146	6,942	0.54	0.36	0.65	0.57	0.06	0.41	0.65	0.36	0.69	0.36	0.41
POPISK	Human	n.a.	n.a.	4,114	2,112	0.68	0.68	0.56	0.62	0.24	0.54	0.70	0.65	0.59	0.65	0.54
PAAQD	Human	n.a.	n.a.	14,059	4,631	0.59	0.49	0.70	0.70	0.17	0.20	0.94	0.64	0.71	0.64	0.20
Repitope	Human	-	62	21,146	6,942	0.77	0.65	0.33	0.70	0.37	0.71	0.69	0.53	0.83	0.53	0.71
Repitope HLA Annot	Human	+	62	21,146	6,942	0.82	0.70	0.35	0.74	0.45	0.77	0.72	0.57	0.86	0.57	0.77
Repitope HLA Rank%	Human	+	62	21,146	6,942	0.79	0.66	0.33	0.71	0.40	0.75	0.68	0.54	0.85	0.54	0.75
Repitope HLA Bind	**Human**	**+**	**62**	**21,146**	**6,942**	**0.79**	**0.66**	**0.35**	**0.72**	**0.41**	**0.70**	**0.73**	**0.56**	**0.83**	**0.56**	**0.70**
Repitope_Feat_75	Human	+	42	21,146	6,942	0.78	0.66	0.35	0.71	0.39	0.71	0.71	0.54	0.84	0.54	0.71
Repitope_Feat_50	Human	+	31	21,146	6,942	0.78	0.65	0.34	0.70	0.38	0.72	0.70	0.54	0.83	0.54	0.72
Repitope_Feat_25	Human	+	14	21,146	6,942	0.76	0.61	0.35	0.69	0.35	0.68	0.70	0.52	0.82	0.52	0.68
Repitope_Clust_80	Human	+	62	19,593	5,956	0.72	0.50	0.27	0.65	0.29	0.73	0.61	0.45	0.84	0.45	0.73
Repitope_Clust_60	Human	+	62	17,356	5,003	0.72	0.47	0.27	0.66	0.28	0.68	0.65	0.44	0.83	0.44	0.68
Repitope_Mouse	Mouse	-	40	8,693	2,089	0.71	0.49	0.26	0.69	0.26	0.59	0.72	0.40	0.85	0.40	0.59
Repitope_Mouse_HumanModel	Mouse	-	62	8,693	2,089	0.60	0.33	0.30	0.53	0.10	0.63	0.50	0.29	0.81	0.29	0.63
Repitope_Primates	Primates	-	12	411	116	0.80	0.66	0.36	0.82	0.54	0.67	0.87	0.67	0.87	0.67	0.67
Repitope_Primates_HumanModel	Primates	-	62	411	116	0.71	0.53	0.39	0.71	0.32	0.55	0.78	0.49	0.81	0.49	0.55

Immunogenicity score ratios of adjacent peptide pairs predict immune transitions

Single amino acid substitutions can drastically affect the immunogenicity of the MHC-bound peptide. Delineating the landscape of "immune transitions," *i.e.*, escaping and epitope formation, is the critical step toward understanding the evolutionary trajectories of microbes and cancer. To this end, we first characterized the 6,175 adjacent peptide pairs identified from our epitope metadataset, of which 940 were transitional pairs based on their annotations. As expected, the ratios of their immunogenicity scores predicted immune transitions, with AUC and the best threshold of 74% and 1.26, respectively (**Figure 4a, b**). Substitutions at anchor positions 2 and 9

156 in nonamers significantly affected the immunogenicity of the mutated counterparts
157 (**Figure 4c**). Moreover, mutating residues K and Y, residues enriched in
158 non-immunogenic MHC binders, significantly augmented immunogenicity (**Figure 2d**
159 and **Figure 4d**). Next, we characterized transitional peptide pairs of the same viral
160 origins (**Figure 4e, f**). Ratios of immunogenicity scores of transitional peptide pairs
161 were significantly higher than those of non-transitional pairs in all of the five viruses
162 analyzed (**Figure 4e**). The combined analysis yielded AUC of 79% (**Figure 4f**). These
163 findings strongly suggested that the viral adaptation trajectory can be predicted from the
164 dynamic changes in immunogenicity scores.

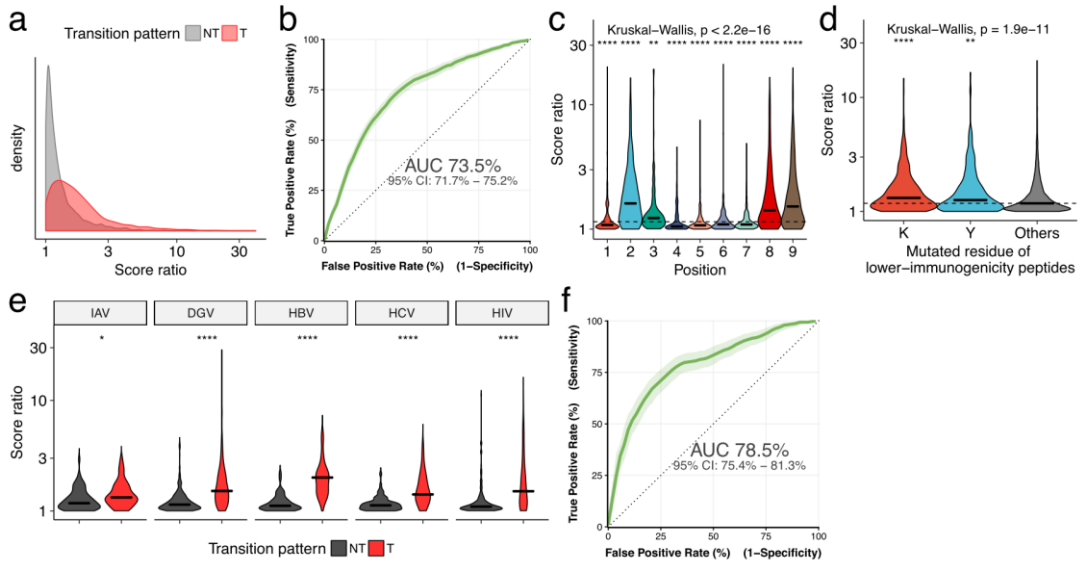

Figure 4. Immune transitions. (a-b) Prediction of immune transitions from the ratios of immunogenicity scores. (c-d) The distributions of immunogenicity score ratios. Gray dashed line indicates the overall median. (e-f) Immune transitions in different viruses. See the legend of **Figure 1d** for data sources. In (c-e), *P* values were calculated by Kruskal-Wallis test followed by Wilcoxon rank sum test with FDR adjustment; **, $p < 0.01$; ****, $p < 0.0001$. NT, non-transitional; T, transitional.

Immune transitional landscapes delineated by epitope mapping in sequence space

Strong immunogenicity does not necessarily mean robust immunogenicity because of potential immune evasion. The discrepancy of these two aspects was exemplified by the neighbor network clustering analysis on an epitope RRYQKSTEL and 132 neighbors (**Figure 5a**). This epitope, whose immunogenicity score was 0.994, was chosen because it has the largest number of neighbors in our metadataset. Indeed, there were 32 non-immunogenic neighbors, forming two clusters. The Cluster 3 consisted of P9 mutants, in which both annotations and predictions fluctuated. In

173 contrast, the Clusters 2, a cluster of P8 mutants, consisted of non-immunogenic peptides
174 with only one exception. These observations indicated that, while P8 mutation deprives
175 the epitope of immunogenicity, P9 mutation undermines the robustness of its
176 immunogenicity, possibly by affecting its binding to restricting HLAs.

177 To gain more comprehensive insights into the immunogenicity landscapes in
178 epitope sequence space, we next conducted *in silico* mutagenesis analysis; we
179 computationally generated all possible neighbors only single amino acid distant from
180 original viral peptides (**Figure 4e, f**). While mean scores were higher in epitopes,
181 coefficients of variance were higher in MHC binders (**Figure 5b, c**). When focusing on
182 the central cluster in neighbor networks, similar but more enhanced trends were
183 observed (**Figure 5d, e**). As for nonamers, P1- and P8-mutating clusters had higher
184 average scores, whereas P2- and P9-mutated clusters had higher score variances,
185 potentially because of disrupted interactions with restricting HLAs (**Figure 5f, g**). We
186 next classified peptides based on their annotated immunogenicity and existence of their
187 adjacent but transitional counterparts. The differences in immunogenicity scores,
188 per-cluster mean scores, and intracluster score variances between transitional and
189 non-transitional peptides were statistically significant (**Figure 5h-j**). Most notably,
190 non-immunogenic but next to immunogenic peptides exhibited higher scores and lower

intracluster score variances than robustly non-immunogenic ones. These observations indicate that increased intracluster variance, as well as decreased immunogenicity score, represents the hallmark of escaping mutations. Our findings may help to choose less escape-prone epitopes for the development of robustly effective vaccines.

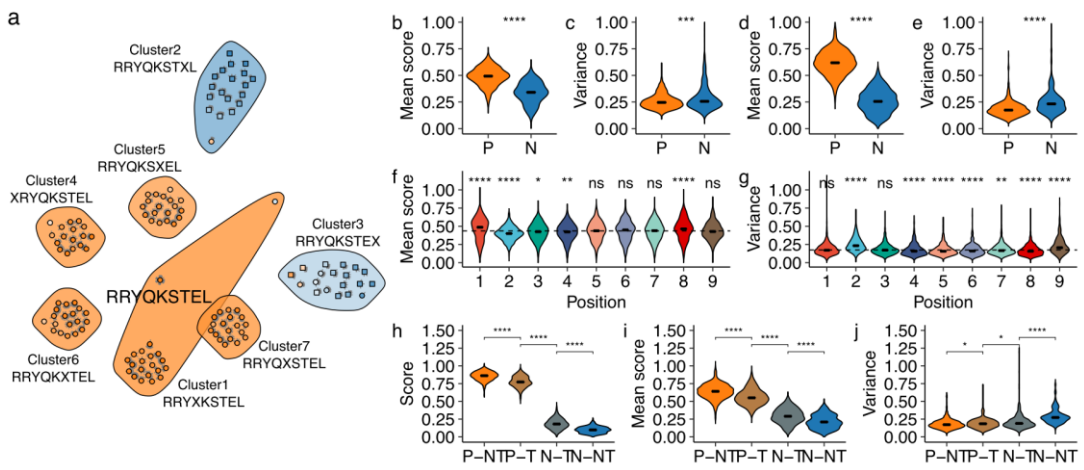

Figure 5. Mapping immune transitional landscapes in sequence space. (a) An example neighbor network. An epitope RRYQKSTEL was chosen as representative. Edges represent single amino acid substitution, weighted by inversed score ratios. Colors indicate predicted immunogenicity scores, and shapes indicate annotated immunogenicity (circle, immunogenic; square, non-immunogenic). A walktrap algorithm was adopted for clustering. Labels indicate consensus sequences for each cluster. (b-c) The mean score and coefficient of variance for the peptide of interest and all *in silico* mutated neighbors. (d-e) The mean score and coefficient of variance for the peptide of interest and neighbors residing in the same cluster. (f-g) Mean scores and variance per cluster stratified by the mutated positions in nonamers. (h-i) Mean scores and variance per cluster stratified by the immunogenicity-transition patterns. Peptides that have at least one transitional neighbors were categorized as transitional. In (b-i), *P* values were calculated by Wilcoxon rank sum test with FDR adjustment; *, $p < 0.05$; **, $p < 0.01$; ***, $p < 0.001$; ****, $p < 0.0001$. P, immunogenic; N, non-immunogenic; NT, non-transitional; T, transitional.

Accumulation of transitional neoepitopes predicts patient survival in checkpoint blockade cohorts

197 Tumor neoepitope burden defined by intracellular processing and MHC binding
198 has been shown to correlate with response and patient survival in various checkpoint
199 blockade cohorts[26–28]. However, neoepitopes that elicit the most prominent and
200 sustained CTL response often remain elusive. Here, we demonstrated that accumulation
201 of transitional neoepitopes successfully identified patients responding favorably to
202 checkpoint inhibitors in melanoma and lung carcinoma cohorts (**Figure 6a**; *P*-value =
203 6.1×10^{-5} in the log-rank test). Unlike the previously proposed neoantigen fitness model[11],
204 this immune transition model predicted overall survivals without any model-specific
205 parameter; predictions can be made from the linear sums of the score ratios. Moreover,
206 our model successfully reduced the total number of neoepitopes without compromising
207 predictive efficacy; the median numbers of neoepitopes were 39 vs. 4 in high- and
208 low-burden groups in our model, considerably small numbers compared to 285 vs. 34.5
209 according to the original criteria (**Figure 6b, c**). These findings place tumor neoepitope
210 biology in a more generalized context of CTL immunity. Larger-scale cancer mutanome
211 profiling study is warranted to validate and further sophisticate the prediction of
212 neoepitope candidates, thus galvanizing research in precision oncoimmunology.

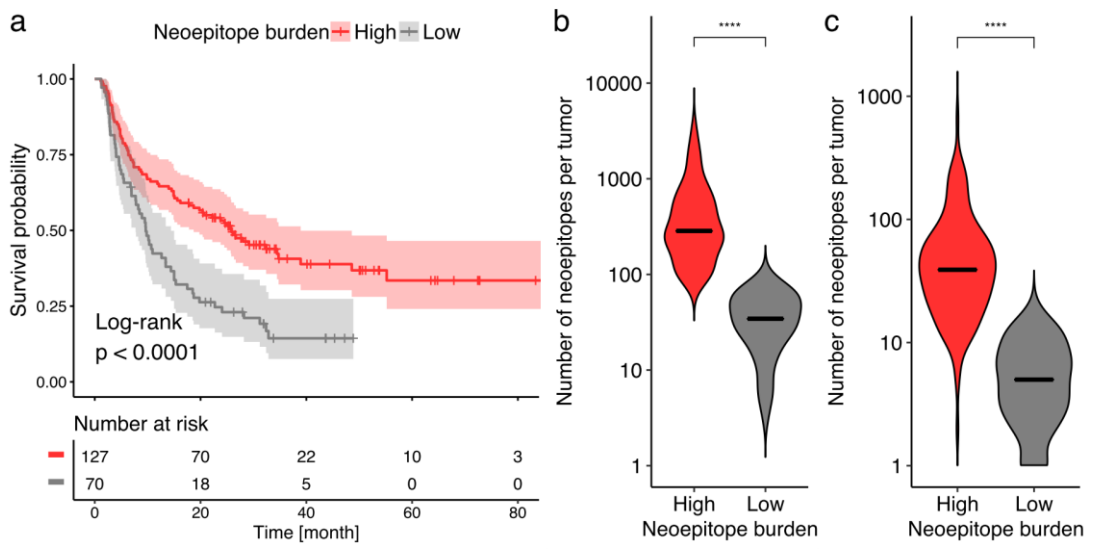

Figure 6. Prediction of survivals of patients treated with checkpoint inhibitors. (a) A Kaplan-Mayer curve. The dataset compiled by Lukzsa *et al*.[11] derived from two melanoma cohorts[27,28] and one lung carcinoma cohort[26] was used. Patients whose sums of score ratios exceed 100 were classified as high neoepitope burden. (b-c) Neoepitope burdens defined by (b) the original criteria[11] and (c) our criteria.

213

Discussion

The ultimate goal of immunogenicity prediction is to predict which peptide best triggers sustained immunological response *in vivo*. In contrast to the complexity of the regulatory mechanisms *in vivo* including regulatory T cells[29], CTL exhaustion mediated through chronic immune checkpoint signals[30], and the immunosuppressive microenvironment engendered by solid tumors[31,32], T cell activation is primarily governed by the MHC-peptide-TCR interactions, with some assistance from coreceptors such as CD8[33]. Considering this asymmetric complexity, T cell activation assay *in vitro* inevitably yields some false positives *in vivo*. That being said, however, eliminating candidates least likely to be immunogenic *in silico* would significantly expedite the research of precision immunotherapy.

Our analysis demonstrates highly accurate immunogenicity predictions *in silico*. Our framework is novel in that it utilizes TCR fragment library as a peptide homology evaluation function from the viewpoint of TCR repertoire, in contrast to previous studies that define homology from sequence-level pairwise alignment scores[11,12]. TCR-peptide contact potential profiling recapitulates the context-dependent effects of single amino acid substitutions on immunogenicity. In contrast to high-throughput *in vitro* T cell assays that only provide estimates of immunogenicity of the peptides tested, our

232 framework can extrapolate the high-dimensional rules of immunogenicity learned from
233 more than 20,000 peptide sequences to delineate the immunogenic landscapes in
234 sequence space. Finally, our framework is advantageous in that it does not depend on the
235 *a priori* knowledge of HLA restrictions, thus enabling *in silico* screening solely from
236 genomic data such as tumor mutation datasets.

237 Escaping is one of the most prominent issues in developing effective vaccines[34,35],
238 and neoepitope formation is a promising target towards tumor-specific therapeutic
239 vaccines[36,37]. These phenomena are two sides of the same coin in sequence space.
240 However, the bidirectional effects of single amino acid substitutions in terms of
241 immunogenicity are likely highly context-dependent and remain barely understood.
242 Even a single mutation could affect various aspects of CTL immunity, including
243 proteolytic processing, transportation to endoplasmic reticulum, stability and structural
244 orientation in MHC presentation, and propensity for TCR recognition[1,9,38]. We found
245 that dynamic changes in immunogenicity scores are predictive of viral escaping and
246 response to checkpoint blockade therapy in cancer patients. Moreover, we characterized
247 the peculiarity of peptides adjacent to transitional boundaries defined from neighbor
248 network architectures in sequence space. To our knowledge, this work is the first
249 attempt to systematically explain the effects of single amino acid substitutions in the

250 context of bidirectional immune transitions.

251 Our study has several caveats and limitations. First, the presumed correlation
252 between the sequence-based contact potential profiles and the real TCR affinity/avidity
253 profiles is not experimentally validated. Although we only utilized TCRβ CDR3
254 sequences from unsorted T cell sources, this point could further be explored in the
255 future. Moreover, since the majority of the epitope data utilized were obtained from
256 microbial sources, the application of the Repitope framework for autoimmunity and
257 oncoimmunology may require further validations and optimizations. Finally, it remains
258 an open question whether similar strategies could reveal underlying rules governing the
259 antigen recognition by helper T cells and regulatory T cells, which if exist would
260 undoubtedly engender a more unified view of T cell biology.

261 In conclusion, our analyses establish a framework for accurate epitope
262 immunogenicity prediction by introducing sequence-based approximation of
263 TCR-peptide contact potential profiles and provide insights into CTL immunogenicity
264 landscapes. Simultaneous prediction of immunogenicity and immune transitional
265 potentials represents a promising strategy toward more effective and less escape-prone
266 precision immunotherapy against infectious diseases and cancer.

267

Methods

MHC-I epitope/ligand dataset

Human data. HLA-I-restricted peptide sequences with known immunogenicity for CTL were collected from public databases [Immune Epitope Database (IEDB, as of Mar 30, 2018)[15], the best-characterized CTL epitopes from Los Alamos National Laboratory (LANL) HIV Sequence Database[18], LANL HCV Sequence Database[17], EPIMHC[16], MHCBN[20], and TANTIGEN[21]] and previous publications[8,9,19]. For the peptides from IEDB database, only those with the evidence listed in **Supplementary Table 2** were considered valid. Peptides presented on non-human MHC molecules were discarded, whereas those presented on HLA class I molecules expressed in non-human hosts (e.g., transgenic mice) were included. Either peptide sequences whose lengths were other than 8, 9, 10, and 11, or those containing non-standard letters were discarded. In this manner, a total of 21,146 unique peptides were identified. A total of 1,872 (8.9%) peptides that had conflicting immunogenicity annotations were identified. In this study, peptides that were annotated as immunogenic in at least one dataset were considered immunogenic. Consequently, 6,942 (32.8%) unique epitopes and 14,204 (67.2%) MHC binders were identified.

Other species. CTL epitopes and MHC binders loaded on species-specific MHC

286 molecules were retrieved from the IEDB database (as of Mar 30, 2018). Species studied
287 were mice and primates (bonobo, chimpanzee, gorilla, marmoset, and rhesus macaque).

288 **Contact potential profiling (CPP)**

289 *Concept*. Immunogenic peptides presented on the MHC class I molecules must be
290 recognized by the TCRs of $CD8^+$ CTLs with strong affinity to trigger subsequent
291 immunological cascades[14]. The entire TCR repertoires do not necessarily recognize
292 those peptides; instead, a quite limited set of epitope-specific TCRs would be sufficient.
293 Moreover, given the flexible conformational changes upon binding between TCR and
294 peptide-MHC complex, it is plausible that only a restricted set of residue pairs between
295 the peptide and the CDR3 loop initially act as a "seed" of molecular scanning that may
296 endow the complex the time for conformational changes to further enhance the affinity
297 and trigger CTL activation[14,39,40]. In this view, the interacting surfaces could be
298 approximated as a pair of linear sequences, and by deconvoluting the TCR repertoire
299 into a set of fragments of a defined amino acid length, the process of molecular
300 scanning could be interpreted as a pairwise sequence alignment problem. One caution is
301 that, although an ordinary sequence alignment algorithm involves a similarity matrix
302 which gives higher values to biochemically similar residue pairs, higher scores must be
303 given to more strongly interacting residue pairs rather than more biochemically similar

304 residue pairs in order to interpret the alignment as the reflection of intermolecular
305 interaction. For this purpose, amino acid pairwise contact potentials (AACPs) were
306 adopted from the AAIndex database[41]
307 (http://www.genome.jp/aaindex/AAindex/list_of_potentials) to generate custom
308 substitution matrices. The Smith-Waterman local alignment algorithm maximizes the
309 alignment score of a given TCR-derived sequence fragment against the whole sequence
310 of a given peptide, and its alignment score can be interpreted as a correlate of the
311 intermolecular contact potential. Consequently, the interactions between a given peptide
312 and a given TCR repertoire can be profiled by summarizing the distribution of
313 alignment scores.

314 *Fragment library*. We hypothesized that human public TCR clonotypes are biased in
315 favor of "publicly" immunogenic peptides rather than non-immunogenic ones, and
316 therefore could be utilized as a probe for immunogenicity. We focused on the CDR3
317 loops because they are primarily responsible for the interactions with MHC-loaded
318 peptides, whereas MHC α-helices are typically contacted with more conserved CDR1
319 and CDR2 loops[1,42,43]. We restricted our analysis to human TCRβ (TRB) repertoire. Due
320 to the frequent lack of annotations of T cell sorting (e.g., $CD8^+$ T cells), we included
321 TCR repertoires from all kinds of T cells. TCR repertoire datasets were collected from

322 NCBI Sequence Read Archive (SRA) and a previous study led by Britanova et al.[44].
323 SRA was searched with the following terms '(T Cell Receptor β) AND human.' The
324 following BioProjects were included: PRJNA389805, PRJNA329041, PRJNA298417,
325 PRJNA273698, PRJNA258001, PRJNA229070, PRJNA79707, and PRJNA79435.
326 Projects in which healthy donors were not involved (e.g., cancer, autoimmune diseases)
327 were omitted. Datasets derived from HIV-infected subjects in the BioProject
328 PRJNA258001 were discarded. Meanwhile, PRJNA316572, involving the unique
329 molecular identifier strategy, were not included in order to maintain consistency in the
330 way of analysis. Fastq files were obtained using fastq-dump script with the following
331 options: --gzip --skip-technical --readids --read-filter pass --dumpbase --split-files --clip
332 --accession [SRA run number]. By using MiXCR software[22], a total of 23,006,555 TRB
333 CDR3 clonotypes were identified. Subsequently, a total of 191,326 clonotypes observed
334 in at least 22 out of 220 (=10%) different datasets were retained as public clonotypes.
335 Finally, the pooled CDR3 sequences were fragmented by a sliding window strategy to
336 generate a fragment library. Sliding windows of amino acid length 3 to 8 were tested.
337 Moreover, since CDR3 loops could interact with peptides in either a forward parallel or
338 antiparallel fashion, reversed CDR3 sequences were simultaneously fragmented and
339 pooled. Resultant fragment pools were compressed to a defined library depth (e.g.,

340 10,000) by random down-sampling while preserving the original proportion of each
341 fragment.

342 *Pairwise sequence alignment*. The *pairwiseAlignment* function implemented in the
343 *Biostrings* package in *Bioconductor*[45] was utilized. This function seeks an optimal
344 alignment which maximizes the overall alignment score defined as a sum of pairwise
345 scores. Alignment type was set "global-local" to obtain an optimal alignment of a CDR3
346 fragment with consecutive subsequences of the peptide. Gaps were not allowed. A set of
347 substitution matrices were generated from a set of thirty-five AACP scales retrieved
348 from the AAIndex database[41]. The scales utilized in this study are summarized in
349 **Supplementary Table 3**. AACP matrices were rescaled so that numerical indicators
350 resided within the range between 0 and 1 for comparative purposes. For analytical
351 purposes, we also prepared inversed AACP matrices (rescaled as well) to mimic the
352 weakest interactions as well as the strongest interactions. A distribution of alignment
353 scores was summarized by calculating representative statistics. Following statistics were
354 utilized: mean, standard deviation, median, 10% trimmed mean, median absolute
355 deviation, skew, kurtosis, standard error, interquartile range, 10% quantile, and, 90%
356 quantile. Predictive features were generated by combining the fragment length, the
357 AACP scale, and the type of statistics. In this manner, a total of 4,620 CPP features

358 were generated for each of the peptides.

359 **Peptide descriptors**

360 Apart from CPP features, sequence-based physicochemical features were also
361 calculated. Each peptide sequence was converted into a set of consecutive fragments of
362 a defined amino acid length, and peptide descriptors were calculated against each of the
363 fragments using functions in the *Peptide* package. Following functions were utilized:
364 *aIndex*, *blosumIndices*, *boman*, *charge*, *crucianProperties*, *fasgaiVectors*, *hmoment*,
365 *hydrophobicity*, *instaIndex*, *kideraFactors*, *mswhimScores*, *pI*, *protFP*, *vhseScales*, and,
366 *zScales*. The distributions of the values were summarized as described in the paragraph
367 of CPP. Moreover, a set of categorical features indicating whether the peptide of interest
368 is free from a specific amino acid residue (e.g., tyrosine) were included. Finally, the
369 length of the peptide was included as a feature as well. In this manner, combined with
370 CPP features, a total of 6,081 features were generated for each of the peptides.

371 **HLA restriction**

372 *Annotation*. Experimental annotations on binding to HLA class I molecules were
373 retrieved from IEDB and other databases. HLA genotypes were converted to supertypes
374 according to the rules from Sidney *et al*.[46] Serotypes were treated *per se*. In this work,
375 supertypes and serotypes were not strictly distinguished and treated as “HLA restriction”

376 in a combined fashion. Annotations of HLA restriction against twelve HLA
377 representatives [A1, A2, A3, A24, A26, B7, B8, B27, B39, B44, B58, and B62] were
378 summarized into a matrix of twelve columns indicating whether the peptide in question
379 was bound to the specified HLA type.

380 *Prediction*. Binding prediction against twelve HLA representatives was performed using
381 NetMHC 4.0[6]. Either predicted rank percentiles or their categorical conversions were
382 summarized in a matrix format as described above. The thresholds of rank percentiles
383 for strong and weak binders were 0.5% and 2%, respectively.

384 **Immunogenicity prediction**

385 *Clustering*. Overrepresentation of peptides sharing high sequence homology could lead
386 to biases in the subsequent analysis. Peptides clustering using IEDB epitope clustering
387 tool[16] followed by random down-sampling was performed to reduce the bias and rule
388 out the possibility of overfitting. A homology threshold of either 60%, 80%, or 100%
389 (*i.e.*, no clustering) was compared.

390 *Preprocessing and feature selection*. An iterative machine learning strategy was
391 employed to find out a restrictive set of predictive features for immunogenicity
392 uniformly applicable to the entire epitope/ligand dataset. First, the dataset was
393 partitioned into training and testing subdatasets in a ratio of 4:1. Second, the training

394 subdataset was centered and rescaled using the *preProcess* function implemented in the
395 *caret* package[47]. Third, highly correlating features were eliminated using the
396 *findCorrelation* function in *caret*. The threshold of correlational coefficients was set to
397 be 0.75. Finally, features were selected based on the importance values calculated using
398 the *randomForestSRC.rfsrc* method implemented in the *mlr* package[48]. The 100 most
399 important features were retained unless otherwise stated. The entire feature selection
400 process was iterated five times with different random seeds. Moreover, considering the
401 possibility that the initial order of features matters in the feature selection process, the
402 same five iterations were performed using the inversely reordered feature set. The
403 testing subdataset was not utilized for feature selection purposes.
404 *Machine learning*. Preliminary experiments suggested that the optimal algorithm is the
405 extremely randomized trees (ERT) with *mtry* and *numRandomCuts* being 35 and 2,
406 respectively. The class imbalance was taken into consideration by inverse weighting.
407 ERT model was trained using the training subdataset. The testing subdataset was
408 preprocessed using the processing function defined by the training subdataset and was
409 subjected to predictions.
410 *Immunogenicity score*. Peptides were divided into five chunks of approximately same
411 sizes. ERT model training and immunogenicity prediction were performed in a

leave-one-chunk-out fashion with a predefined set of the most predictive features. HLA binding data from either experimental annotations or predictions by NetMHC 4.0 was incorporated as features when indicated. The entire prediction process (data splitting, preprocessing, and machine learning) was iterated five times with different random seeds. The estimated probability values were averaged for each of the peptides. We termed the averaged probability of immunogenicity as "immunogenicity score." We extrapolated this framework to an external dataset by applying the twenty-five ERT models to the entire external dataset.

Immune transition

Concept. Single amino acid substitutions have multifaceted effects on the immunogenicity of epitopes and MHC binders. Loss of immunogenicity is called escape or immune evasion. Also, the term immunoediting is used particularly in the field of cancer[49]. In this work, we unify the terminology as "escape." For the sake of simplicity, we do not take other mechanisms of evasion such as impaired intracellular antigen processing, somatic loss of HLA heterozygocity[50,51], and checkpoint-mediated CTL exhaustion and apoptosis[52]. In contrast, there is no appropriate terminology for the acquisition of immunogenicity. In this work, we refer to this phenomenon as "epitope/neoepitope formation." Escaping and epitope formation can be understood as

two sides of the same coin in sequence space. Therefore, we defined a more unified concept, "immune transition," in this work, which is defined as a change in immunogenicity between a pair of MHC-presented peptides with just one edit distance. By definition, the immune transition is bidirectional.

Neighbor network analysis. A graph network was constructed from a set of peptides, where pairs of peptides with one edit distance were considered edges. The low-to-high score ratios were considered edge distances, and edges were weighted by the inversed score ratios. Network clustering was performed using the *cluster_walktrap* function implemented in the *igraph* package[53]. The consensus sequence per cluster was generated using the ClustalW algorithm implemented in the *msa* package[54] in *Bioconductor*[45].

In silico mutagenesis analysis. To delineate the immunogenicity landscape in a broader context, we computationally expand neighbor networks by simulating the immunogenicity scores of computationally single amino acid substituted peptides. Simulated peptides with indels were not generated. Note that we ignore the possibility that the artificially introduced mutation could potentially affect factors outside the MHC-peptide-TCR axis such as altered proteolytic degradation. Instead, our primary attention is on exploring the effects of those mutations on MHC presentation and TCR

448 recognition.

449 **Viral escaping analysis**

450 Viral epitopes and MHC binders were retrieved from the IEDB database (as of
451 Mar 30, 2018). Five viruses, namely, influenza A virus (IAV), dengue virus (DGV),
452 hepatitis B virus (HBV), hepatitis C virus (HCV), and human immunodeficiency virus
453 type I (HIV) were analyzed. In virus-specific escaping analyses, only peptide pairs
454 derived from the same viral species with one edit distance were considered transitional.

455 **Tumor neoepitope analysis**

456 The compiled dataset of predicted tumor neoepitopes and clinical annotations by
457 Luksza *et al*.[11] was utilized. These data were derived from two melanoma cohorts and
458 one lung carcinoma cohort treated with anti-PD-1 and anti-PD-1 checkpoint inhibitors,
459 respectively[26–28]. The score ratios of mutant peptides relative to their wild-type
460 counterparts were calculated and summed up per patient. The best threshold minimizing
461 the *P*-value by the log-rank test was explored using all cohorts combined. The optimal
462 threshold was 100. Therefore, tumors whose sums of score ratios exceeded this
463 threshold were classified as “high neoepitope burden.”

464 **Computational analysis**

465 Main computational analyses were conducted using R ver. 3.4.4

466 (https://www.r-project.org/) [55]. The latest versions of R packages were consistently used.

467 Key datasets and essential in-house functions were bundled as the R package *Repitope*,

468 which is publicly distributed in GitHub (https://github.com/masato-ogishi/Repitope/).

469 Other scripts are available upon request.

470 **Statistics**

471 All statistical analysis is exploratory; no predetermined experimental protocols

472 were applied before initiating the entire project. All data inclusion and exclusion criteria

473 were described in the above sections. No accounting for missing data values is applicable.

474 Non-parametric hypothesis testing was employed unless otherwise stated. *P*-values were

475 adjusted for multiple comparisons on the basis of false discovery rate (FDR) unless

476 otherwise stated. All statistical analyses were conducted in R.

477

Acknowledgments

We thank Dr. Couture-Cossette and Dr. Ueno for the valuable advice.

Funding: This work is not supported by any external funding sources.

Author contributions: M.O. designed the study, performed computational analyses, and drafted the manuscript; M.O. and H.Y. wrote the manuscript.

Competing interests: The authors declare no competing interests.

Data availability: Both the datasets compiled and the custom functions are available as the R package *Repitope* on GitHub (https://github.com/masato-ogishi/Repitope/). Other analytical scripts are available at the GitHub repository and also available upon request.

488 # References

489 1. Rudolph, M. G., Stanfield, R. L. & Wilson, I. A. How TCRs bind MHCs,
490 peptides, and coreceptors. *Annu. Rev. Immunol.* **24,** 419–66 (2006).
491 2. Sette, A. *et al.* The relationship between class I binding affinity and
492 immunogenicity of potential cytotoxic T cell epitopes. *J. Immunol.* **153,** 5586–92
493 (1994).
494 3. Schmidt, J. *et al.* In silico and cell-based analyses reveal strong divergence
495 between prediction and observation of T-cell-recognized tumor antigen T-cell
496 epitopes. *J. Biol. Chem.* **292,** 11840–11849 (2017).
497 4. Duan, F. *et al.* Genomic and bioinformatic profiling of mutational neoepitopes
498 reveals new rules to predict anticancer immunogenicity. *J. Exp. Med.* **211,** 2231–
499 2248 (2014).
500 5. Stranzl, T., Larsen, M. V., Lundegaard, C. & Nielsen, M. NetCTLpan:
501 pan-specific MHC class I pathway epitope predictions. *Immunogenetics* **62,** 357–
502 368 (2010).
503 6. Andreatta, M. & Nielsen, M. Gapped sequence alignment using artificial neural
504 networks: application to the MHC class I system. *Bioinformatics* **32,** 511–517
505 (2016).

506 7. Editorial. The problem with neoantigen prediction. *Nat. Biotechnol.* **35,** 97–97
507 (2017).
508 8. Calis, J. J. A. *et al.* Properties of MHC Class I Presented Peptides That Enhance
509 Immunogenicity. *PLoS Comput. Biol.* **9,** (2013).
510 9. Chowell, D. *et al.* TCR contact residue hydrophobicity is a hallmark of
511 immunogenic CD8 + T cell epitopes. *Proc. Natl. Acad. Sci.* **112,** E1754–E1762
512 (2015).
513 10. Zhang, W. *et al.* Accurate prediction of immunogenic T-cell epitopes from
514 epitope sequences using the genetic algorithm-based ensemble learning. *PLoS*
515 *One* **10,** e0128194 (2015).
516 11. Luksza, M. *et al.* A neoantigen fitness model predicts tumour response to
517 checkpoint blockade immunotherapy. *Nature* **551,** 517–520 (2017).
518 12. Balachandran, V. P. *et al.* Identification of unique neoantigen qualities in
519 long-term survivors of pancreatic cancer. *Nature* **551,** 512–516 (2017).
520 13. Rasmussen, M. *et al.* Pan-Specific Prediction of Peptide–MHC Class I Complex
521 Stability, a Correlate of T Cell Immunogenicity. *J. Immunol.* **197,** 1517–1524
522 (2016).
523 14. Tian, S., Maile, R., Collins, E. J. & Frelinger, J. A. CD8+ T Cell Activation Is

524 Governed by TCR-Peptide/MHC Affinity, Not Dissociation Rate. *J. Immunol.*
525 **179,** 2952–2960 (2007).
526 15. Vita, R. *et al.* The Immune Epitope Database 2.0. *Nucleic Acids Res.* **38,** (2009).
527 16. Reche, P. A., Zhang, H., Glutting, J. P. & Reinherz, E. L. EPIMHC: A curated
528 database of MHC-binding peptides for customized computational vaccinology.
529 *Bioinformatics* **21,** 2140–2141 (2005).
530 17. Kuiken, C., Yusim, K., Boykin, L. & Richardson, R. The Los Alamos hepatitis C
531 sequence database. *Bioinformatics* **21,** 379–384 (2005).
532 18. Llano, A., Williams, A., Olvera, A., Silva-Arrieta, S. & Brander, C.
533 Best-Characterized HIV-1 CTL Epitopes: The 2013 Update. *HIV Mol. Immunol.*
534 *2013* 3–25 (2013).
535 19. Tung, C. W. *et al.* POPISK: T-cell reactivity prediction using support vector
536 machines and string kernels. *BMC Bioinformatics* **12,** 446 (2011).
537 20. Lata, S., Bhasin, M. & Raghava, G. P. S. MHCBN 4.0: A database of MHC/TAP
538 binding peptides and T-cell epitopes. *BMC Res. Notes* **2,** 61 (2009).
539 21. Olsen, L. R. *et al.* TANTIGEN: a comprehensive database of tumor T cell
540 antigens. *Cancer Immunol. Immunother.* **66,** 731–735 (2017).
541 22. Bolotin, D. A. *et al.* MiXCR: software for comprehensive adaptive immunity

542 profiling. *Nat. Methods* **12,** 380–381 (2015).

543 23. Nelson, R. W. *et al.* T Cell Receptor Cross-Reactivity between Similar Foreign

544 and Self Peptides Influences Naive Cell Population Size and Autoimmunity.

545 *Immunity* **42,** 95–107 (2015).

546 24. Keskin, O., Bahar, I., Badretdinov, A. Y., Ptitsyn, O. B. & Jernigan, R. L.

547 Empirical solvent-mediated potentials hold for both intra-molecular and

548 inter-molecular inter-residue interactions. *Protein Sci.* **7,** 2578–2586 (1998).

549 25. Bjerregaard, A. M. *et al.* An analysis of natural T cell responses to predicted

550 tumor neoepitopes. *Front. Immunol.* **8,** 1–9 (2017).

551 26. Rizvi, N. A. *et al.* Mutational landscape determines sensitivity to PD-1 blockade

552 in non-small cell lung cancer. *Science (80-.).* **348,** 124–128 (2015).

553 27. Snyder, A. *et al.* Genetic Basis for Clinical Response to CTLA-4 Blockade in

554 Melanoma. *N. Engl. J. Med.* 2189–2199 (2014). doi:10.1056/NEJMoa1406498

555 28. Van Allen, E. M. *et al.* Genomic correlates of response to CTLA-4 blockade in

556 metastatic melanoma. *Science (80-.).* **350,** 207–211 (2015).

557 29. Wojciech, L. *et al.* The same self-peptide selects conventional and regulatory

558 CD4+ T cells with identical antigen receptors. *Nat. Commun.* **5,** 5061 (2014).

559 30. Attanasio, J. & Wherry, E. J. Costimulatory and Coinhibitory Receptor Pathways

560 in Infectious Disease. *Immunity* **44,** 1052–1068 (2016).

561 31. Eil, R. *et al.* Ionic immune suppression within the tumour microenvironment

562 limits T cell effector function. *Nature* **537,** 539–543 (2016).

563 32. Chang, C. H. *et al.* Metabolic Competition in the Tumor Microenvironment Is a

564 Driver of Cancer Progression. *Cell* **162,** 1229–1241 (2015).

565 33. Luescher, I. F. *et al.* CD8 modulation of T-cell antigen receptor–ligand

566 interactions on living cytotoxic T lymphocytes. *Nature* **373,** 353–356 (1995).

567 34. Goulder, P. J. R. & Watkins, D. I. HIV and SIV CTL escape: implications for

568 vaccine design. *Nat. Rev. Immunol.* **4,** 630–640 (2004).

569 35. Bowen, D. G. & Walker, C. M. Mutational escape from CD8+ T cell immunity:

570 HCV evolution, from chimpanzees to man. *J. Exp. Med.* **201,** 1709–14 (2005).

571 36. Ott, P. A. *et al.* An immunogenic personal neoantigen vaccine for patients with

572 melanoma. *Nature* (2017). doi:10.1038/nature22991

573 37. Hu, Z., Ott, P. A. & Wu, C. J. Towards personalized, tumour-specific, therapeutic

574 vaccines for cancer. *Nat. Rev. Immunol.* **18,** 168–182 (2017).

575 38. Neefjes, J., Jongsma, M. L. M., Paul, P. & Bakke, O. Towards a systems

576 understanding of MHC class I and MHC class II antigen presentation. *Nat. Rev.*

577 *Immunol.* **11,** 823–836 (2011).

578 39. Boniface, J. J., Reich, Z., Lyons, D. S. & Davis, M. M. Thermodynamics of T
579 cell receptor binding to peptide-MHC: evidence for a general mechanism of
580 molecular scanning. *Proc Natl Acad Sci U S A* **96,** 11446–11451 (1999).
581 40. Zhong, S. *et al.* T-cell receptor affinity and avidity defines antitumor response
582 and autoimmunity in T-cell immunotherapy. *Proc. Natl. Acad. Sci.* **110,** 6973–
583 6978 (2013).
584 41. Kawashima, S. *et al.* AAindex: Amino acid index database, progress report 2008.
585 *Nucleic Acids Res.* **36,** 202–205 (2008).
586 42. Garcia, K. C., Teyton, L. & Wilson, I. A. Structural basis of T cell recognition.
587 *Annu. Rev. Immunol.* **17,** 369–97 (1999).
588 43. Cole, D. K. *et al.* T-cell Receptor (TCR)-peptide specificity overrides
589 affinity-enhancing TCR-major histocompatibility complex interactions. *J. Biol.*
590 *Chem.* **289,** 628–638 (2014).
591 44. Britanova, O. V. *et al.* Age-Related Decrease in TCR Repertoire Diversity
592 Measured with Deep and Normalized Sequence Profiling. *J. Immunol.* **192,**
593 2689–2698 (2014).
594 45. Gentleman, R. C. *et al.* Bioconductor: open software development for
595 computational biology and bioinformatics. *Genome Biol.* **5,** R80 (2004).

596 46. Sidney, J., Peters, B., Frahm, N., Brander, C. & Sette, A. HLA class I supertypes:
597 A revised and updated classification. *BMC Immunol.* **9,** 1–15 (2008).
598 47. Kuhn, M. Building Predictive Models in *R* Using the caret Package. *J. Stat. Softw.*
599 **28,** 1–26 (2008).
600 48. Bischl, B. *et al.* mlr: Machine Learning in R. *J. Mach. Learn. Res.* **17,** 1–5
601 (2016).
602 49. Efremova, M. *et al.* Targeting immune checkpoints potentiates immunoediting
603 and changes the dynamics of tumor evolution. *Nat. Commun.* **9,** (2018).
604 50. McGranahan, N. *et al.* Allele-Specific HLA Loss and Immune Escape in Lung
605 Cancer Evolution. *Cell* 1259–1271 (2017). doi:10.1016/j.cell.2017.10.001
606 51. Chowell, D. *et al.* Patient HLA class I genotype influences cancer response to
607 checkpoint blockade immunotherapy. *Science (80-.).* **4572,** eaao4572 (2017).
608 52. Pardoll, D. M. The blockade of immune checkpoints in cancer immunotherapy.
609 *Nat. Rev. Cancer* **12,** 252–264 (2012).
610 53. Csárdi, G. & Nepusz, T. The igraph software package for complex network
611 research. *InterJournal* **Complex Sy,** 1695 (2006).
612 54. Bodenhofer, U., Bonatesta, E., Horejš-Kainrath, C. & Hochreiter, S. msa: an R
613 package for multiple sequence alignment. *Bioinformatics* **31,** btv494 (2015).

55. R Core Team. R: A Language and Environment for Statistical Computing. (2016). doi:ISBN 3-900051-07-0

Supplementary Figures

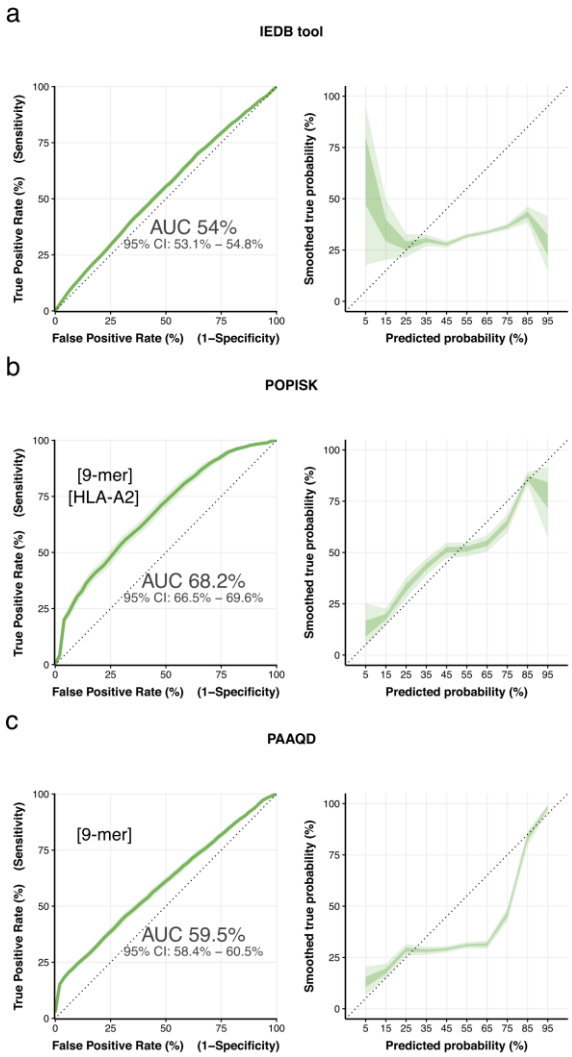

Supplementary Figure 1. Immunogenicity prediction using previously published tools. Immunogenicity was predicted using (a) Immune Epitope Database (IEDB) class I prediction tool, (b) POPISK, and (c) PAAQD. (b-c) POPISK and PAAQD analyses were restricted to HLA-A2-restricted nonamers and nonamers of any HLA restriction, respectively.

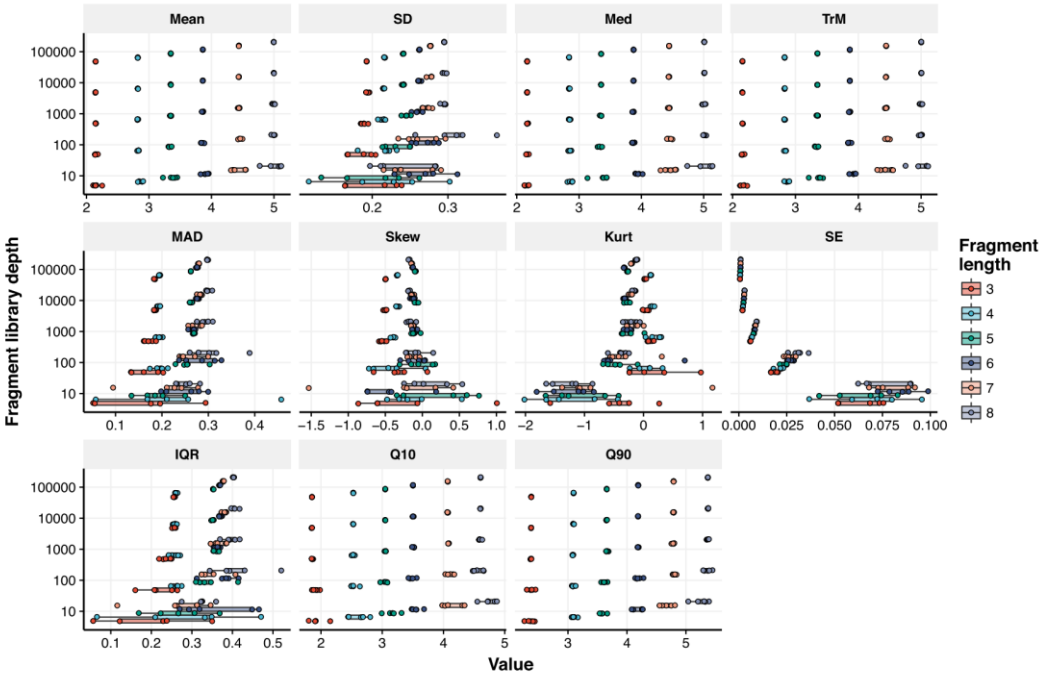

Supplementary Figure 2. Increased fragment library depths reduced variability in CPP feature calculation. The result of epitope RRYQKSTEL using AACP scale KESO980101 was plotted as an example. Calculations were iterated five times with different random seeds. A depth of 10,000 was sufficient to calculate representative statistics with minimal variability between iterations. SD, standard deviation; Med, median; TrM, 10% trimmed mean; MAD, median absolute deviation; Skew, skewness; Kurt, kurtosis; SE, standard errors of mean; IQR, interquartile range; Q10, 10% quantile; Q90, 90% quantile.

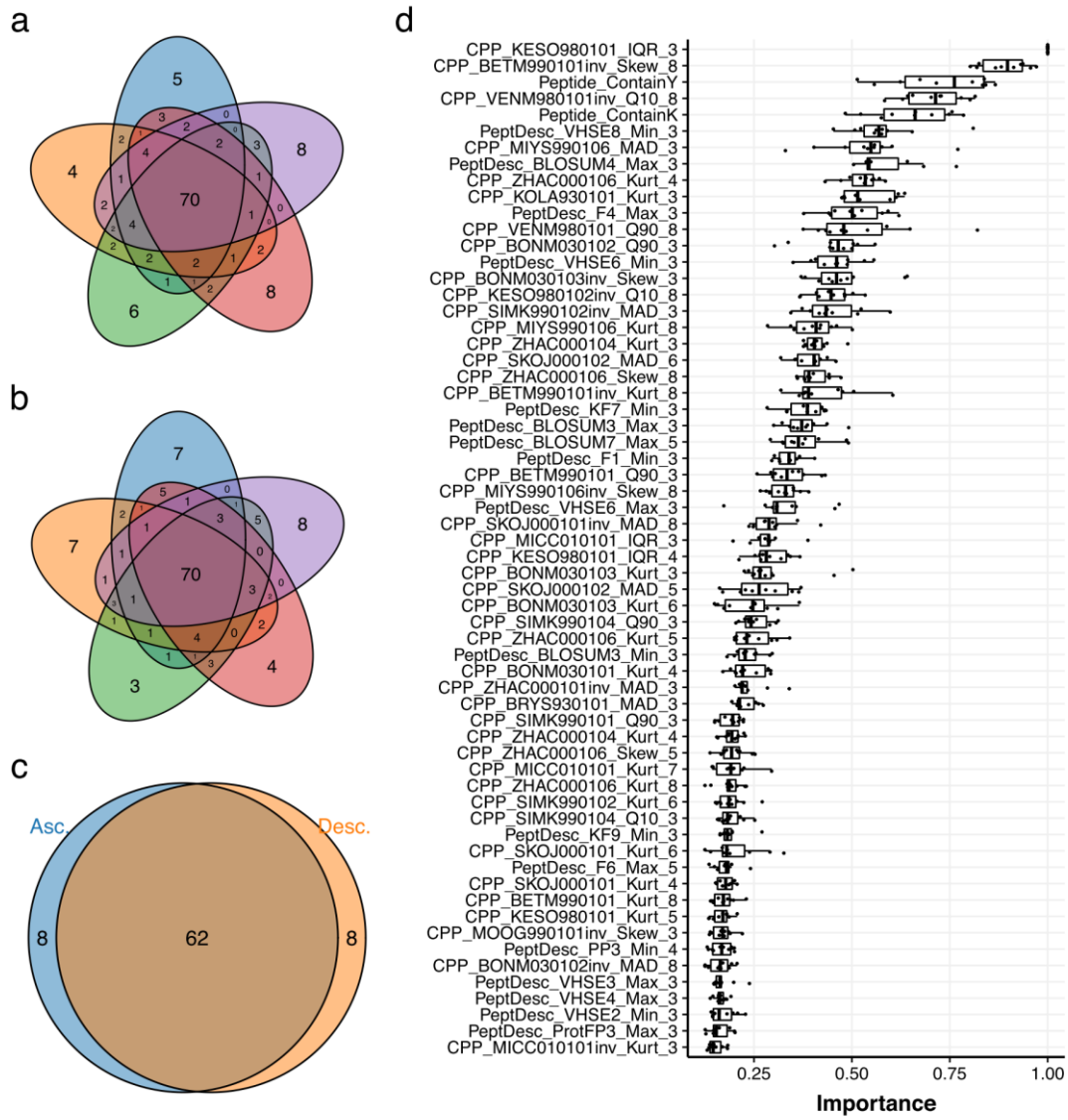

Supplementary Figure 3. Iterative feature selection. Feature importance was calculated by constructing random forest models using 80% of the dataset, and 100 the most important features were retained. Calculations were iterated five times with different random seeds. (a-b) Shared features in five iterations. In the phase of importance calculation, random forest models were trained with a set of features whose names were sorted in (a) an ascending order, and (b) a descending order, respectively. (c) Shared features between ascending vs. descending consensus feature sets. (d) The distributions of importance values for the 62 the most predictive features. See **Methods** for the nomenclature of the features.

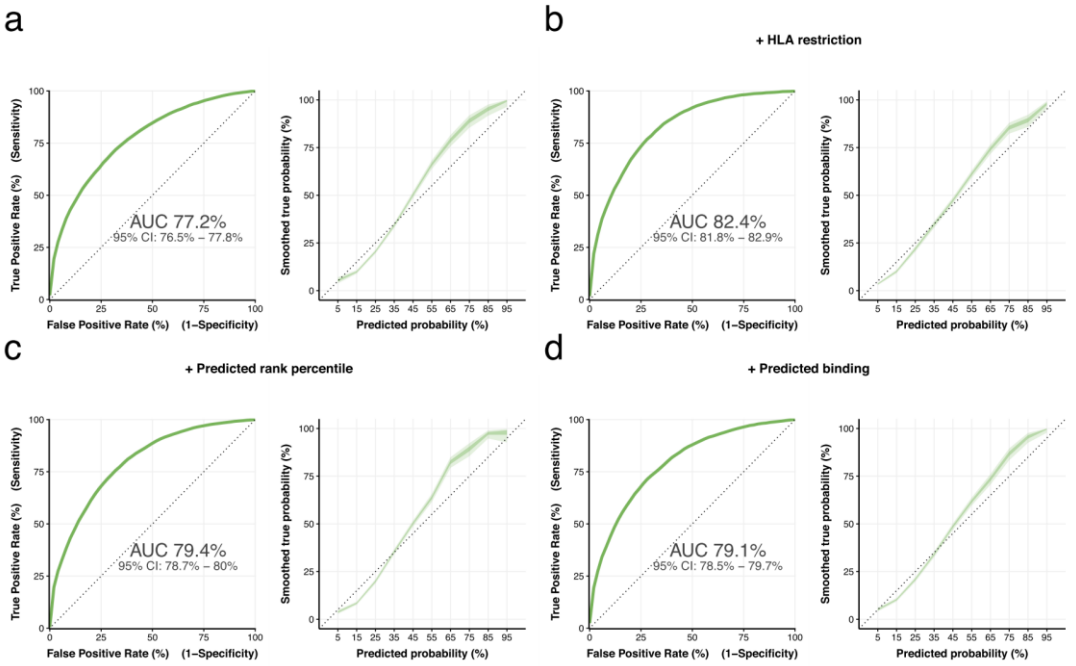

Supplementary Figure 4. The effects of HLA binding information for immunogenicity prediction. (a) Prediction without HLA information. (b) Prediction with annotation-based HLA restrictions. (c-d) Predictions with either (c) rank percentiles or (d) binding categories predicted by NetMHC 4.0 against twelve HLA representatives. Note that (d) depicts the same probabilities as in **Figure 3a**.

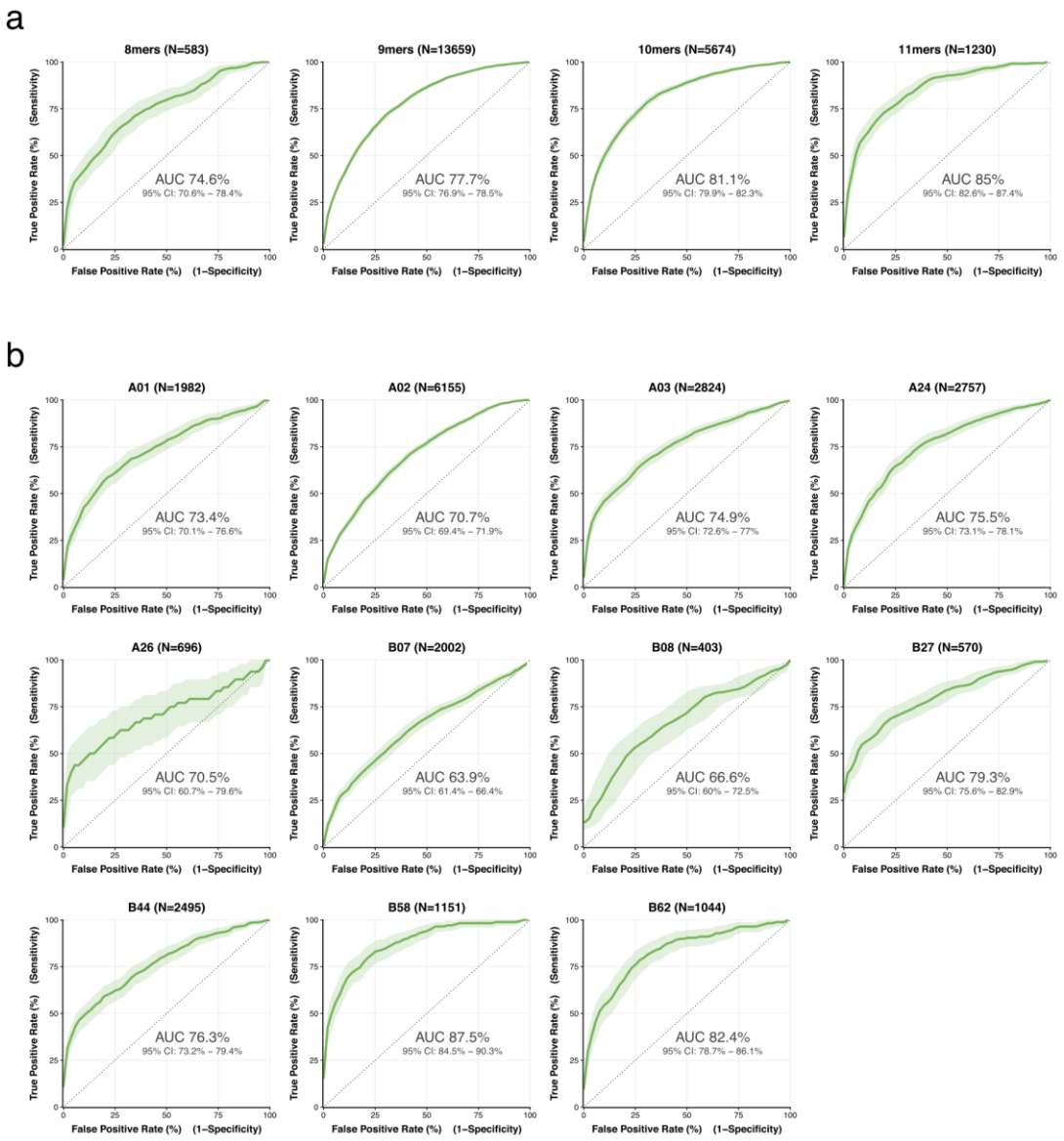

Supplementary Figure 5. Predictive performance of immunogenicity scores stratified by (a) peptide lengths, or (b) restricting HLA supertypes.

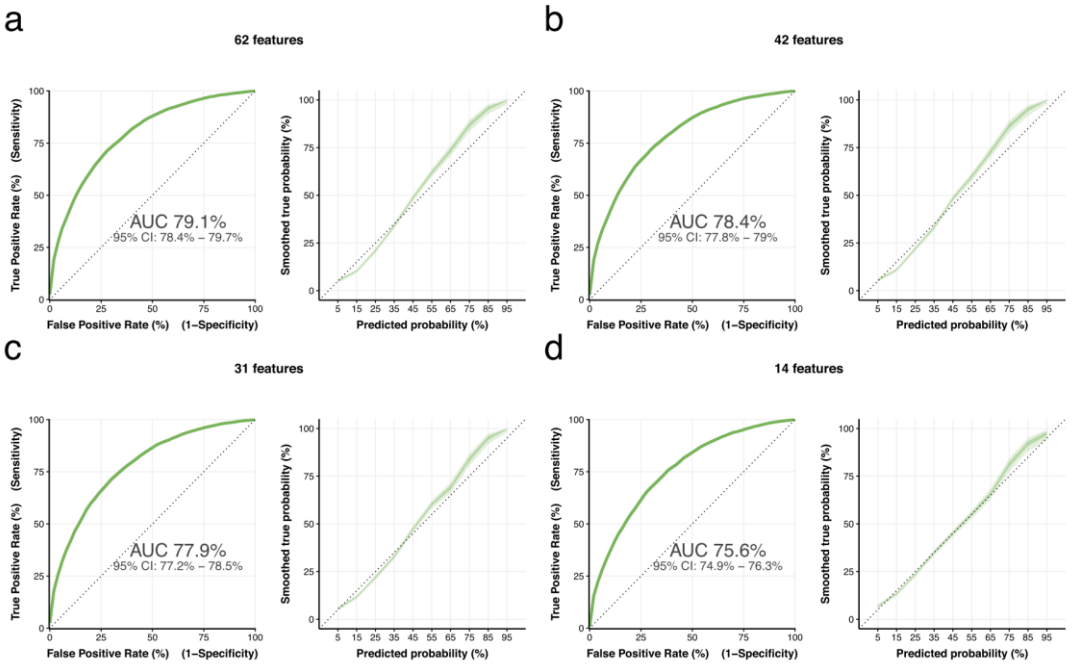

Supplementary Figure 6. The effects of the number of features for immunogenicity prediction. Feature importance was calculated, and the most predictive features were selected as described in **Supplementary Figure 3** and **Methods**. The numbers of features retained in each iteration were (a) 100, (b) 75, (c) 50, and (d) 25. The numbers of features retained after feature selection steps and thus used for model training were indicated on top of each plot. Note that (a) is the same as **Figure 3a**.

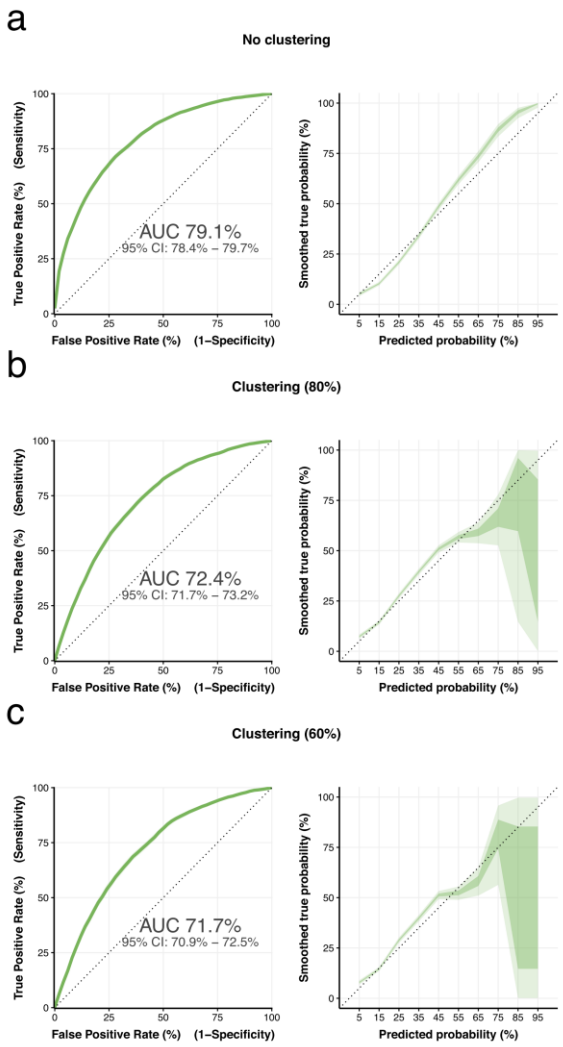

Supplementary Figure 7. The effects of sequence-level peptide homology for immunogenicity prediction. Peptides were clustered using the IEDB clustering tool. (a) No clustering (same as **Figure 3a**). (b-c) Clustering with the similarity threshold of (b) 80% and (c) 60%, respectively.

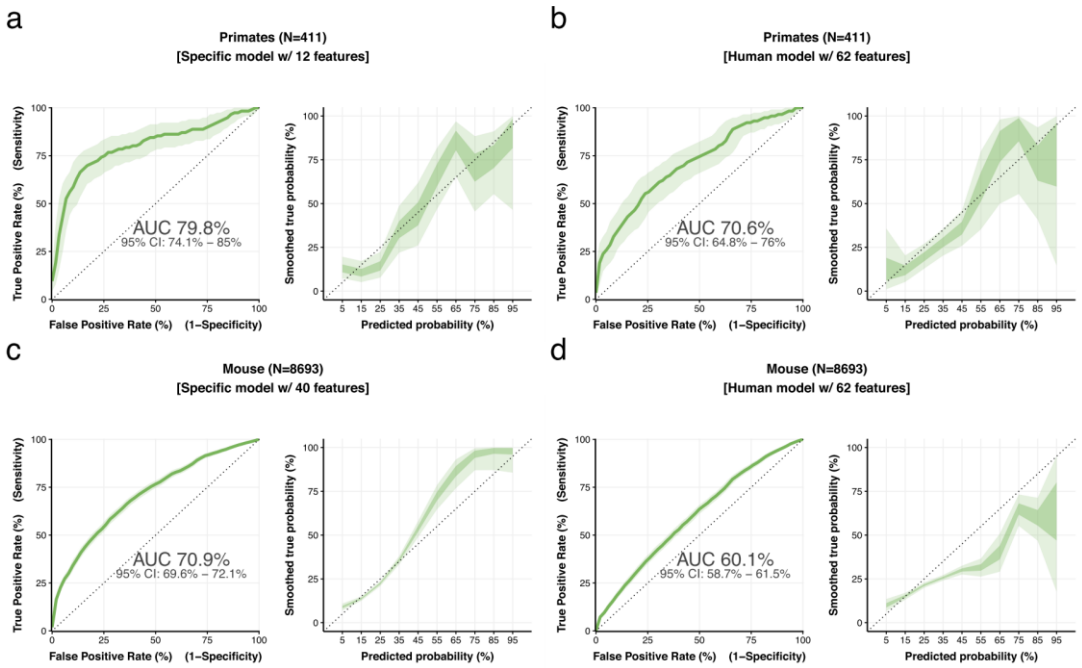

Supplementary Figure 8. Immunogenicity prediction for peptides restricted to the MHC molecules of other species. Peptide information was retrieved from the IEDB database. MHC information was not utilized for model construction. Peptides presented on (a-b) primate and (c-d) mouse MHCs were subject to the immunogenicity prediction. In (a) and (c), dataset-specific models were constructed, whereas in (b) and (d), the models constructed from the human peptide dataset (N=21,146) were extrapolated.

633

Supplementary Tables

Supplementary Table 1. The list of HLA genotype-supertype conversion rules derived from Sidney *et al*.[46]

(A CSV file)

Supplementary Table 2. The list of allowed evidence of immunogenicity for the IEDB dataset.

(A CSV file)

Supplementary Table 3. The list of amino acid pairwise contact potential (AACP) scales utilized in this study.

(A CSV file)